Influence of optical thickness and hot electrons on Rydberg spectra of Ne-like and F-like copper ions

K. B. Fournier
Lawrence Livermore National Laboratory, P. O. Box 808, L-41, Livermore, California 94550

A. Ya. Faenov, T. A. Pikuz, and I. Yu. Skobelev
Multicharged Ions Spectra Data Center of VNIIFTRI, Moscow 141570, Russia

V. S. Belyaev, V. I. Vinogradov, A. S. Kyrilov, and A. P. Matafonov
Central Research Institute of Machine Building, 4, Pionerskaya Street, Korolev, Moscow Region 141070, Russia

I. Bellucci, S. Martellucci, and G. Petrocelli
INFM—Dipartimento di Scienze e Tecnologie Fisiche ed Energetiche, Università di Roma Tor Vergata, Via di Tor Vergata, 00133 Roma, Italy

T. Auguste, S. Hulin, P. Monot, and P. D'Oliveira
Commissariat à l'Energie Atomique, Centre d'Etudes de Saclay, DRECAM, Service de Photons Atomes et Molécules, Bâtiment 522, 91191 Gif-Sur-Yvette, France

(Received 12 September 2002; published 10 January 2003)

Spectra in the 7.10 to 8.60 Å range from highly charged copper ions are observed from three different laser-produced plasmas (LPPs). The LPPs are formed by a 15-ns Nd:glass laser pulse (type I: $E_{\text{pulse}}=1-8$ J, $\lambda=1.064$ μm), a 1-ps Nd:glass laser pulse (type II: $E_{\text{pulse}}=1$ J, $\lambda=1.055$ μm), and a 60-fs Ti:sapphire laser pulse (type III: $E_{\text{pulse}}=800$ mJ, $\lambda=790$ nm). The spectra of high-n ($n\leqslant 14$) transitions in highly charged copper ions, Cu^{19+} to Cu^{21+}, are recorded with a high energy resolution ($\lambda/\Delta\lambda=3000-8000$) spectrometer using a spherically bent mica or quartz crystal. Collisional-radiative models are computed for the emission from each plasma. The sensitivity of the model spectra to opacity effects and to populations of superthermal electrons is studied. For the type I LPPs, opacity effects, treated with escape factors, are necessary to get the correct relative intensities of high-n ($n=5$, 6) Ne-like Cu^{19+} emission features. In the case of the type II LPPs, the contrast between the laser prepulse and the main pulse has been varied from low, $I_{\text{main}}/I_{\text{pp}}=7\times10^{4}$, to high, $I_{\text{main}}/I_{\text{pp}}=3.8\times10^{7}$. For plasmas from low contrast shots, we find good agreement between the observed spectra and optically thin simulations with bulk electron temperatures $T_{\text{bulk}}=0.4$ keV and a small population of superthermal electrons ($T_{\text{hot}}=5.0$ keV) that is $f_{\text{hot}}\leqslant10^{-5}$ of the bulk electron population. For high-contrast type II LPPs, we find higher densities and a combination of $f_{\text{hot}}\sim10^{-5}$ and escape factors best describes the data. For the type III 60-fs LPPs, a population of superthermal electrons ($T_{\text{hot}}\approx5$ keV) that is $\approx5\times10^{-5}$ of the bulk electron population ($T_{\text{bulk}}\approx0.2$ keV) is required to reproduce the observed spectra. The effect of both escape factors and hot electrons in the CR models is to increase the ionization balance and dramatically increase the number of strong lines for each ion considered. We have studied both opacity effects and hot-electron influence on high-n transitions of highly charged Ne-, F-, and O-like ions.

DOI: 10.1103/PhysRevE.67.016402 PACS number(s): 52.38.−r, 32.30.Rj, 52.25.Os

I. INTRODUCTION

The development of methods to create and diagnose hot, dense plasmas is of great interest for many applications including inertial confinement fusion [1] and the interaction of matter with short laser pulses [2–4]. Plasmas with thermal electron distributions with temperatures of hundreds of eV are produced over scales of tens of nanometers by the interaction of short duration (tens to hundreds of fs) laser pulses with solid density matter [5,6]. Populations of hot electrons are known to be produced [7,8] by several nonlinear absorption mechanisms such as resonant absorption [9], vacuum heating [10], and forward scattering instabilities in the strongly driven regime [11]. The presence of a preformed plasma can strongly enhance the production of hot electrons [12,13]. Hot electrons created during the interaction of subpicosecond, high-intensity lasers with both solid targets and clusters of atoms in gas jets have significant effects on the x-ray radiative properties of the produced plasmas. These effects have been studied extensively in recent years. Previous spectroscopic work has noted the effect of beams of hot electrons on the *K*-shell spectra of light ions in pulsed power experiments [14,15] and laser produced plasmas (LPPs) [16–18]. A two-temperature plasma model with a low-temperature Maxwellian electron distribution function (EDF) and a small hot electron fraction (10^{-5}–10^{-3}) at a much higher energy has been successful in describing *K*-shell emission spectra from solid Mg and Al laser targets [14,16]. A two-temperature model with small fractions of hot electrons (10^{-7}–10^{-5}) has been successful in describing *K*-shell

emission spectra from laser-irradiated Ar gas jets [17,19–21] and plasma focus devices [15]. These studies have demonstrated that hot electrons drive the ionization balance to higher charge states [15] and augment the intensity of inner-shell satellite lines [16]. Very recently, the effect of hot electrons on the spectral shape of $4\rightarrow 2$ *L*-shell transitions in near-neonlike krypton ions following the irradiation of clusters of krypton atoms with a high-intensity, subpicosecond laser has been quantified [22]. In the present paper, we look in detail at the kinetics of higher-*n* ($n\geqslant 5$) Rydberg lines of Ne-, F-, and O-like copper ions.

The interaction of low to moderate intensity lasers ($I=10^{10}$ to 10^{14} W/cm^2) with solid targets is well understood [9]. The present work does not address issues with laser-energy deposition processes or target-heat conduction processes. Rather, this work uses high-resolution spectroscopy of *L*-shell x-ray spectra to illustrate the sensitivity of diagnostic simulations to various issues such as plasma ion self-absorption of line radiation and the sensitivity to populations of high-energy electrons beyond the bulk, Maxwellian electron distribution. The spectrum of high-*n* transitions in Ne-, Na-, F-, and O-like ions has a complicated structure; we have done a separate work to identify and classify these transitions [23]. In the present work, we investigate in detail the influence of optical thickness and hot electrons on the kinetics model for spectral intensities. Using multiple laser facilities, we vary laser-flux density by changing the energy and spot size of the laser focus. This allows us to obtain different plasma conditions and helps not only to discriminate between the lines of different charge states, but in some cases, to illuminate different population channels and to see more clearly which spectral lines start to appear with increasing flux density and decreasing laser-pulse duration. Specifically, we look at copper emission spectra from plasmas formed by lasers with $I\approx 10^{11}$–10^{12} W/cm^2, with $I\approx 10^{14}$–10^{16} W/cm^2, and with $I\approx 10^{18}$ W/cm^2 (which we designate type I, II, and III, respectively—they are described in detail in Secs. II and V). We demonstrate that for the type I LPPs, the escape factor description of opacity effects is required for high-*n* members of the Ne-like Rydberg series. For the type II and type III LPPs, we find that populations of multi-keV electrons that are small fractions ($f=10^{-6}$–10^{-5}) of the bulk electron population ($T_{\mathrm{bulk}}=0.2$–0.3 keV) are necessary to reproduce the observed data. There is some evidence that the type II spectra also exhibit opacity effects.

This paper is structured as follows. In Sec. II the laser systems creating the three types of plasmas studied and the targets used are presented. In Sec. III our atomic kinetics model is presented, along with a description of the atomic data that are input. In Sec. IV the analysis of the model sensitivity to changes in electron temperature and density, to optical depths, and to the presence of hot electrons is studied. In Sec. V, opacity effects on type I plasmas, the diagnosis of very high-*n* spectra in type II LPPs, and an analysis of hot electrons in a type III LPP spectrum are presented. In Sec. VI, a discussion of this work and other recent, related work is presented. A summary of our results is given in Sec. VII.

II. EXPERIMENT DESCRIPTION

Three laser installations have been used for measurements of x-ray spectra from copper plasmas. The first set of experiments (so-called type I) was carried out in the Tor Vergata University of Roma (Italy) where plasma was produced using the fundamental output wavelength of a Nd:glass laser, 1.055 μm, in a vacuum chamber, which has a pressure of 10^{-2} mbar. The laser source was a Quantel Nd:glass laser delivering pulses with a maximum energy of 20 J and a temporal duration of 12–15 ns. It consisted of a chain of two Nd:YAG (YAG, yttrium aluminum garnet) and two Nd:glass amplifiers. The repetition rate was limited to 1 shot/min to minimize the thermal lens effect. A 20 cm focal-length doublet lens focused the laser beam on the target at a 45° angle of incidence. The estimated beam diameter at the focal point was 300 μm. In our experiments the laser energy was varied between 1–8 J. The resulting intensity on target for type I experiments is 10^{11}–10^{12} W/cm^2.

The second set of experiments (type II) were carried out on the ''Neodym'' laser facility [24] at the Central Research Institute of Machine Building near Moscow. The laser energy was up to 1.0 J, and the pulse duration in these experiments was kept to 1 ps. The fundamental wavelength of the Nd:glass laser was used. The laser pulses were focused into a focal spot with diameter within the range of 100 to 900 μm, yielding a peak intensity within the range from 10^{14} to 10^{17} W/cm^2. In such a setup there are two types of prepulses before the main pulse. The first prepulse arises from amplified spontaneous emission in the regenerative amplifier. This prepulse occurs for about 8 ns before the main pulse and has ≈ 0.3 mJ of energy, such that the intensity contrast, $I_{\mathrm{main}}/I_{\mathrm{pp}}$ (the peak intensity to prepulse intensity ratio) is about 1.3×10^7. In our experiments we did not change this prepulse. The second prepulse arises from the many pass regime of amplification in the regenerative amplifier and the finite transmission of Pockel cells. This prepulse occurs for about 13 ns before the main pulse and had duration of pulse equal to 1 ps. In the type II experiments we changed the intensity of this prepulse: ''low contrast''—the intensity contrast is about 7×10^4 and ''high contrast''—the intensity contrast is about 3.8×10^7.

In the upper panel of Fig. 1, two picosecond ($I=10^{16}$ W/cm^2) LPP spectra produced with high (middle) and low (bottom) ratios of the main pulse to the prepulse peak intensities are shown. The $2p$-nd and $2s$-np Ne-like transitions are indicated with the standard notation. There is little obvious difference between the two type II spectra. Shown for comparison is a high-intensity ($I=10^{12}$ W/cm^2) spectrum from the type I experiments, there are fewer lines from higher charge states (Cu^{20+} and Cu^{21+}) in the type I spectrum. Shown in the lower panel of Fig. 1 is a comparison between two LPP spectra from the type II experiments in which the focusing lens has been moved from best focus (middle) to a 1 mm displacement (bottom). This results in a lower plasma temperature in the bottom trace, as is demonstrated by the diminished F-like Cu^{20+} ion features. Also shown is a low-intensity spectrum from the type I experiments. The same reduction in signal from lines of the ions

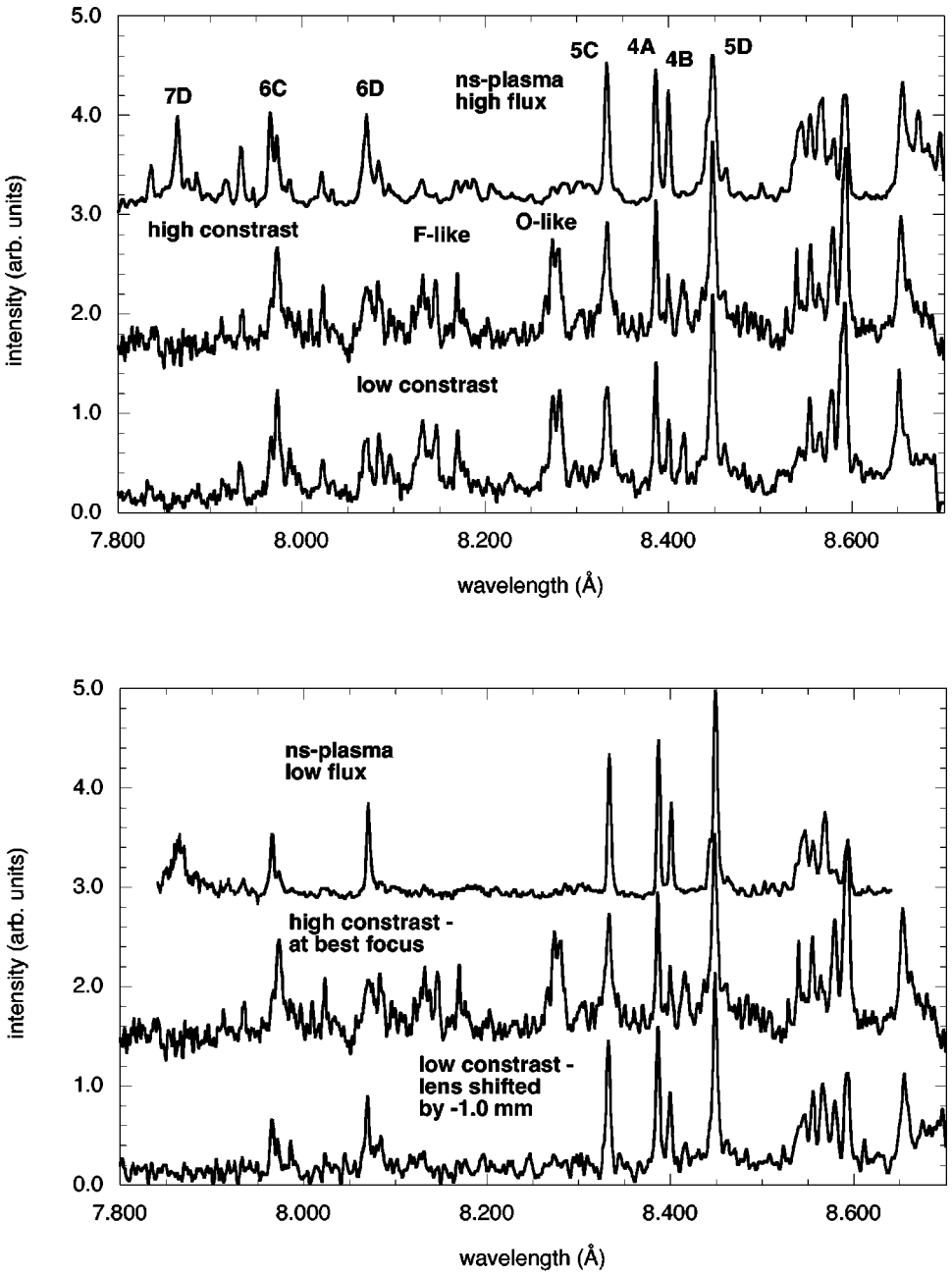

FIG. 1. (Upper) Two ps-pulse LPP spectra recorded with high and low contrast between the main laser pulse and the prepulse. Both spectra are for the laser at best focus. Also shown is a high-intensity 15-ns-pulse LPP spectrum. (Lower) Two ps-pulse LPPs, both with high contrast between the main pulse and the prepulse, and with the laser at best focus and with the lens moved 1 mm from best focus. Also shown is a low-intensity 15-ns-pulse LPP spectrum.

more highly charged than the Ne-like Cu^{19+} is seen comparing the type I traces in the upper and lower panels of Fig. 1.

The third set of experiments (type III) was performed with the Saclay (France) 10-TW laser (UHI10), which was designed to generate 60-fs pulses at a 10-Hz repetition rate [25]. It employs the standard chirped pulse amplification (CPA) [26,27] technique. Ti:sapphire rods are used as the lasing medium and the operating wavelength of the system is 790 nm. In order to produce such high-power ultrashort pulses with a good contrast, first, the low-energy ultrashort pulse is stretched up to 300 ps by an aberration free Offner stretcher. The pulse energy is about 1.8 J after four stages of amplification. Then the compression is performed in a vacuum chamber directly connected to the experimental chamber. The contrast, measured with a high dynamic cross correlator, is about 10^{-5} at 1 ps, and about 10^{-7} at several ns. The total energy in the laser pulse is about 800 mJ. The 80-mm-diameter laser beam was focused with an $f/2.35$ off-axis parabolic mirror onto copper targets, which were placed at a 22.5° angle from the direction of the incident laser beam. The focal spot diameter measured in vacuum was about 30 μm, giving a laser intensity on the target in the 10^{18} W/cm^2 range.

In a recent work, we have identified in detail the copper ion line features in the 7.50 to 8.70 Å range [23]. In that paper, we describe the accuracy of our wavelength calibrations and the energy resolution for the same spectrometer setup [28–30] used here in the Nd:glass experiments. Based on systematic variation of laser pulse energy, we identified the high-n Rydberg lines of the Ne-like spectrum as well as high-n Na-like satellite transitions and lines from the more highly charged F- and O-like ions. The calculated dominant

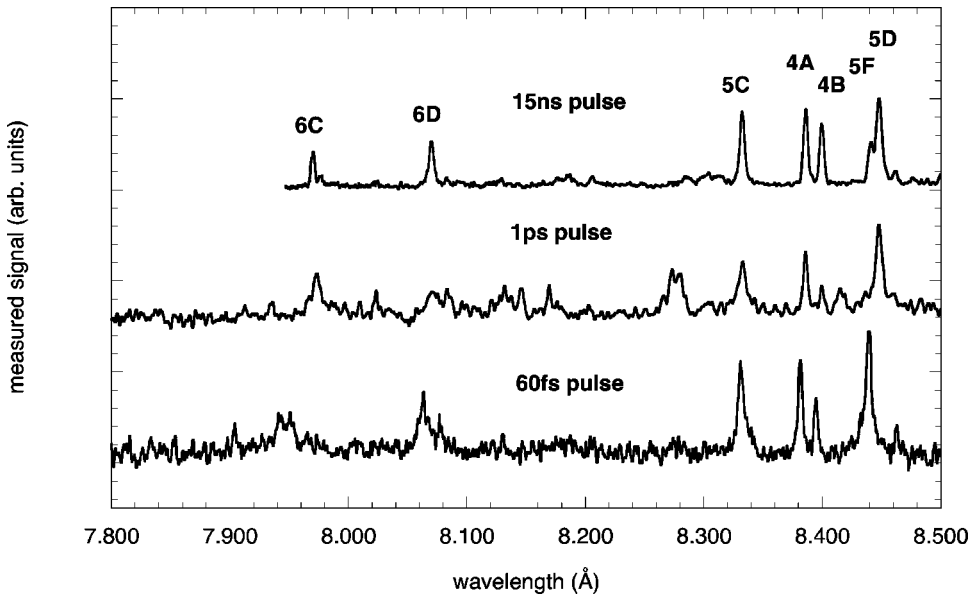

FIG. 2. Nd:glass LPP spectra: type I (lens shifted 5 mm from best focus) and type II (1-ps laser pulse), and a type III Ti:sapphire (60-fs laser pulse) LPP spectrum. Evidence of hot electrons is visible in the ps and fs LPPs.

jj-basis state for the upper level of each observed transition is given in our paper; the labels given in Tables II–V of Ref. [23] are used to identify spectral features in the figures that follow. Figure 2 contrasts data taken in the type I, II, and III experiments for laser intensities of $\approx 7\times 10^{10}$, 10^{16}, and 10^{18} W/cm^2, respectively. In the case of the 1-ps experiment, the contrast between the main pulse and the prepulse was in the high regime ($\approx 10^7$). Enhancement of F-like Cu^{20+} ion features in the type II and III spectra is evidence of hot electron populations, this will be discussed in Sec. V.

In the type I and II experiments, a stepped target was used; one part of the target contained cooper, while the second part contained NaF, Mg, or Al, which produced spectral lines used for reference wavelengths. The height of the steps was 300–800 μm. Between laser shots, the target was moved in the plane perpendicular to the laser beam to obtain spectra of the material investigated and reference materials on the same spectrograph film. The target step served to physically separate the two spectral images on the film. The type III (60 fs) experiments did not have the calibration lines on the same film as the Cu spectra, thus there is a larger uncertainty in the position of the observed lines in the copper data from the Saclay experiments. Each target was used for 1–10 shots in Nd:glass laser experiments, and 200 shots in Ti:sapphire laser experiments.

III. KINETICS CALCULATIONS

In what follows, we simulate the observed line intensities for high-*n* Rydberg lines in near-neonlike ions (Mg-like Cu^{17+} to O-like Cu^{21+}) using a steady-state collisional-radiative model. The ion kinetics that give rise to the observed emission account for the effects of hot electron populations on collisional excitation and ionization rate coefficients, and opacity effects on the strength of individual lines. A recent work [22] on the *L*-shell spectra of Kr ions illuminated by long (ns scale) and short (60 fs) duration laser pulses reaches a similar conclusion to what we find in the present work. That is, the opacity effects in the model are necessary to reproduce the observed relative strengths of line features in the long pulse spectra from solid targets, and that a population of multi-keV hot electrons is necessary to reproduce the distribution of charge states seen in the short-pulse spectra.

Line intensities from the data in the present work have been compared with synthetic spectra calculated using atomic data from the HULLAC package [31–33]. Figure 3 shows the synthetic collisional-radiative (CR) spectra for Mg- to O-like Cu^{17+} to Cu^{21+} in the 7.1 to 8.6 Å range. The energy levels and radiative transition rates, along with autoionization rates [34], are calculated by RELAC [31,32]. All levels with principal quantum number $n\leqslant 9$ have been allowed to interact in the calculation of the structure and rates for each ion. Electron impact excitation collision cross sections between all levels of each ion are computed semirelativistically in the distorted wave approximation using RELAC's multiconfiguration wave functions by the technique of Bar-Shalom, Klapisch, and Oreg [33]. Collisional excitation rate coefficients are found by averaging the collisional cross sections over a Maxwellian electron velocity

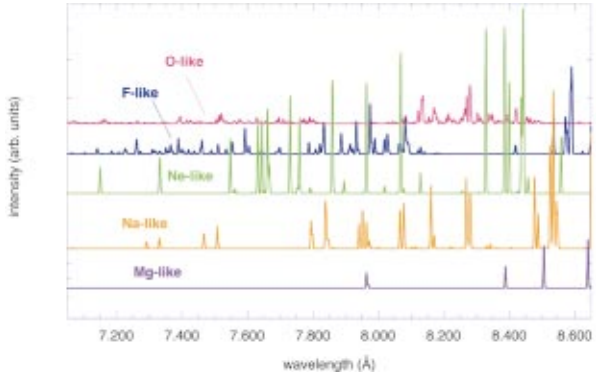

FIG. 3. (Color) Collisional-radiative spectra for Mg-, Na-, Ne-, F-, and O-like (bottom to top) Cu ions. The calculation has $T_e = 250$ eV, $N_e = 10^{21}$ cm^{-3}, and escape factors calculated for an assumed plasma diameter $L = 50$ μm.

distribution at either the bulk ($T_{\rm bulk}$ or T_e) or hot ($T_{\rm hot}$) electron temperature. Direct ionization rate coefficients [35,36] and photoionization cross sections [37], have been computed from all fine-structure energy levels. The rates of the inverse three-body and radiative recombination processes have been found by detailed balance of the forward rate at the bulk temperature. The rate coefficient for radiationless capture (leading to dielectronic recombination) into the levels of the Mg-, Na-, and Ne-like ions has been found by detailed balance of the corresponding autoionization rate.

All level energies and rate coefficients have been entered into the CR rate matrix for the Cu ions of the present work, and the resulting steady state level populations are then found according to

$$\frac{dn_j}{dt}=0=\sum_{i\neq j} n_i R_{i,j}-n_j\sum_{i\neq j} R_{j,i}, \tag{1}$$

where n_j is the population in level j, and $R_{i,j}$ is the rate at which population leaves level i and goes to level j, possibly belonging to a neighboring ion. The resulting intensity for an observed line is given by

$$I_{j,i}=n_j A_{j,i}, \tag{2}$$

where $A_{j,i}$ is the radiative transition rate.

We assume a bi-Maxwellian distribution to account for the effects of hot electrons on collisional excitation and ionization. That is, we assume a bulk Maxwellian electron distribution represented by temperature $T_{\rm bulk}$ and a second, much smaller Maxwellian electron distribution represented by $T_{\rm hot}$. The Maxwell-Boltzmann probability of finding an electron in the energy range E to $E+dE$ is given by

$$P(E,T_e)dE=\frac{2E^{1/2}}{\pi^{1/2}(k_B T_e)^{3/2}}\exp\left(\frac{-E}{k_B T_e}\right)dE, \tag{3}$$

where k_B is the Boltzmann constant. The rate coefficient γ for an electron impact transition at some temperature T_e is given by averaging the energy dependent cross section for the reaction over the distribution of electron velocities,

$$\gamma(T_e)=\int_{E_{\rm th}}^{\infty} v\,\sigma(E)P(E,T_e)dE, \tag{4}$$

where $E_{\rm th}$ is the threshold energy for the transition and $v=\sqrt{2E/m}$. The *effective* rate coefficient for electron impact excitation or ionization is given by

$$\Xi=(1-f_{\rm hot})\,\gamma(T_{\rm bulk})+f_{\rm hot}\,\gamma(T_{\rm hot}), \tag{5}$$

where Ξ is in cm^3 s^{-1}, γ is the rate coefficient for either process at the specified temperature, and $f_{\rm hot}$ is the ratio of the number in the hot distribution to the number in the hot and bulk distributions,

$$f_{\rm hot}=\frac{N_e(T_{\rm hot})}{N_e(T_{\rm bulk})+N_e(T_{\rm hot})}. \tag{6}$$

For the present work, we have computed synthetic spectra with $f_{\rm hot}=10^{-7}$, 5×10^{-7}, 10^{-6}, 2×10^{-6}, 3×10^{-6}, 5×10^{-6}, 10^{-5}, 2×10^{-5}, and 5×10^{-5}. Above 10^{-6}, the response of the F- and O-like ions in the simulation is sensitive to the value of $f_{\rm hot}$.

We have included the effects of plasma self-absorption in our steady-state level population calculations with escape factors [38,39] on the radiative decay rates

$$A^{\rm eff}=\epsilon A_{j,i}, \tag{7}$$

where $A^{\rm eff}$ is the effective transition rate in the presence of photon trapping and ϵ is the escape factor that depends on the atomic mass, the ion temperature, and the plasma radius. For this work, we assume an isothermal, spherical plasma with a diameter ranging from 30 to 150 μm and an ion temperature $T_{\rm ion}=\frac{2}{3}T_e$ or T_e, for computing thermal broadening contributions to each transition's line width. We find that the choice of ion temperature has almost no effect on the computed self-absorption in each synthetic spectrum. Photon trapping redistributes the level population in the considered ions, particularly enhancing the population in the upper levels of strong transitions. The altered level populations mean that the absorption is different; the calculation is iterated until a self-consistent solution for the escape factors is reached. The enhanced level populations are redistributed by collisions, and in some cases, significantly enhance the emission in previously weak lines (discussed below).

IV. MODEL SENSITIVITIES

A. Electron temperature and density

Figure 4 shows T_e dependence in the CR spectra for highly charged copper ions. The average copper-ion charge increases as T_e goes from 200 to 500 eV from 18.76 to 20.70, thus going from a fraction of an electron in the M-shell to an average charge state that is dominated by O-like Cu^{21+}. This is reflected in Fig. 4 as the F- and O-like lines become more prominent with increasing temperature. By $T_e=400$ eV, the characteristic Ne-like lines are less prominent than features composed of multiple strong F- and O-like transitions.

Figure 5 shows the electron-density dependence in the CR spectra for highly charged copper ions in the N_e range of interest to the present work.

As the electron density goes from 10^{20} to 5×10^{21} cm^{-3}, the average ion charge increases from 18.81 to 19.27 for fixed $T_e=250$ eV. As the density increases above 5×10^{21}, the model predicts that recombination is strongly enhanced and the average ion charge actually drops again, reaching 18.84 at 5×10^{22} cm^{-3}. Above $N_e=5\times10^{21}$ cm^{-3}, the populations in the levels of the Ne- and F-like ions are near to local thermodynamic equilibrium with the levels of the ground configuration of the F- and O-like ions, respectively. The only visible effect of changing density in Fig. 5 is an enhancement at high density of high-energy ($\lambda<8.1$ Å) F-like features that make up a weak background.This is due to strong three-body and radiative recombination from the O-like ion.

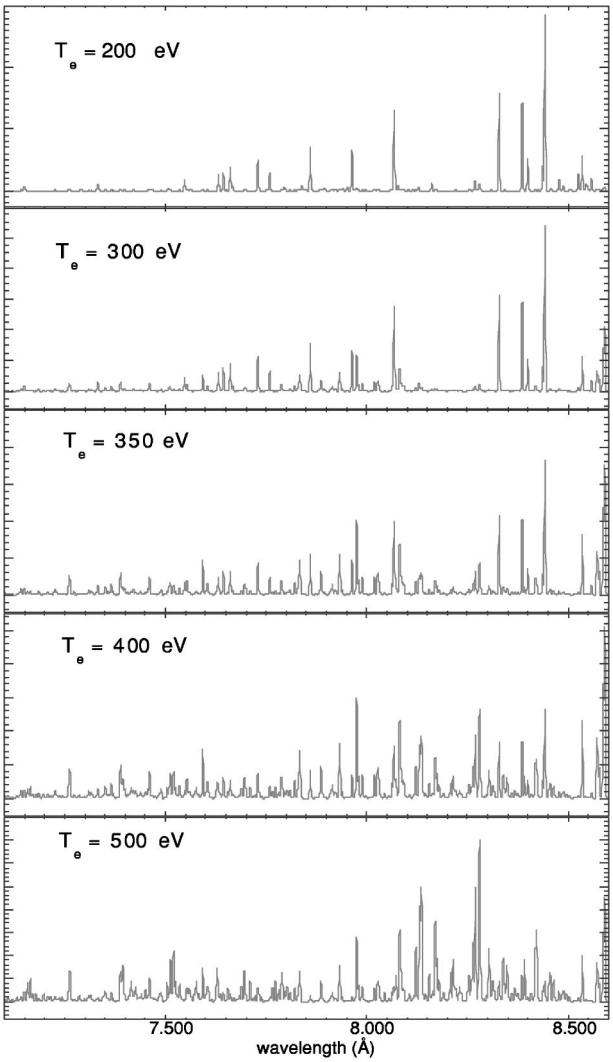

FIG. 4. Optically thin CR spectra for Mg-, Na-, Ne-, F-, and O-like Cu ions computed for $N_e = 10^{21}$ cm^{-3} and different electron temperatures. Each line feature has been given a Gaussian profile with a 3.0 *m*Å FWHM.

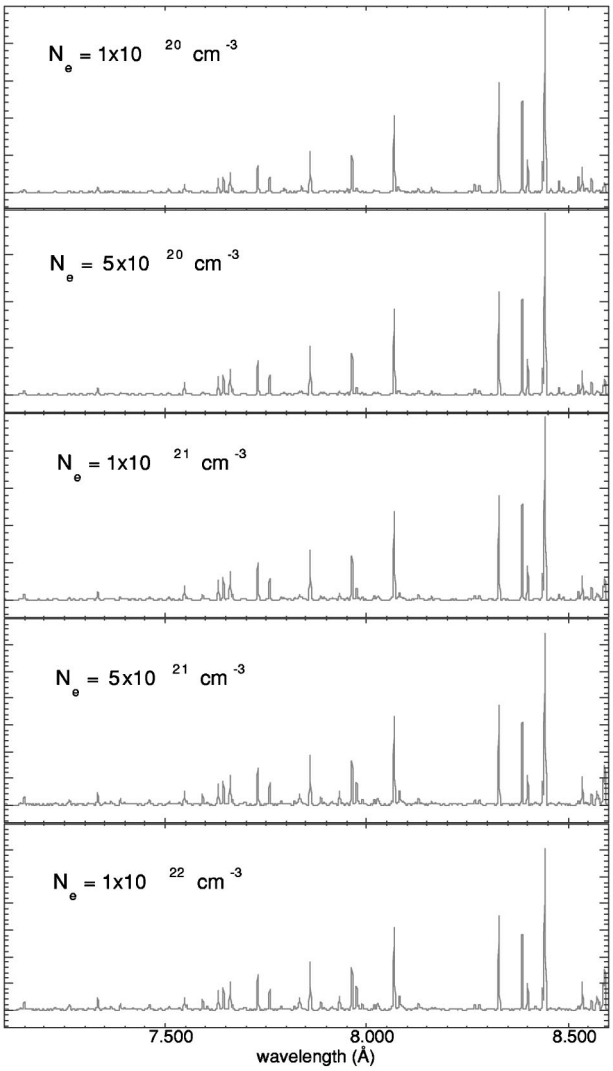

FIG. 5. Optically thin CR spectra for Mg-, Na-, Ne-, F-, and O-like Cu ions computed for $T_e = 250$ eV and different electron densities. Each line feature has been given a Gaussian profile with a 3.0 mÅ FWHM.

B. Optical depths

The relative intensities of nC and nD lines in Ne-like ions are used as diagnostics of both temperature and density in many plasmas [40]. For high-density plasmas, it is essential to account for self-absorption of neonlike line radiation in order to calculate accurately the ratios of diagnostic lines. Figure 6 shows the dependence on optical depth, as represented by escape factors, for the CR calculations by varying the assumed plasma diameter, L. The most obvious effect of the escape factors is to reduce the strength of the $5D$ line relative to the $4A$, $4B$, and $5C$ lines, and to reduce the strength of $6D$ relative to $6C$. The inclusion of the optical depths in the simulations also shifts the calculated ionization balance significantly higher, from $\langle Z \rangle = 19.10$ in the optically thin case (middle panel of Fig. 5) to $\langle Z \rangle = 19.56$ in the $L = 150$ μm calculation, and the fractions of F- and Ne-like ions go from 0.207 to 0.522 and 0.664 to 0.376, respectively. This is due to increased ionization from excited levels with enhanced population in the models with escape factors. Reducing the assumed plasma diameter for the escape factor calculation reduces the enhancement of the population in excited levels, and thus the total rate of ionization, as seen in Fig. 6.

Another effect seen in the simulations with escape factors is that the nF and nG lines are strikingly enhanced. Partly, this is a relative increase since the nC and nD lines are more strongly absorbed than the corresponding nF and nG lines. There is also an absolute enhancement due to collisional transfer of population in the $2p^5nd$ levels to the $2p^5ns$ upper levels of the nF and nG transitions. The population in the $2p^5nd$ upper levels of the nC and nD transitions is greatly enhanced ($\sim \times 4$ for $L = 100$ μm) because the escape factor in Eq. (7) suppresses the drain channels from these levels, thus creating a source for enhancing the nF and nG lines.

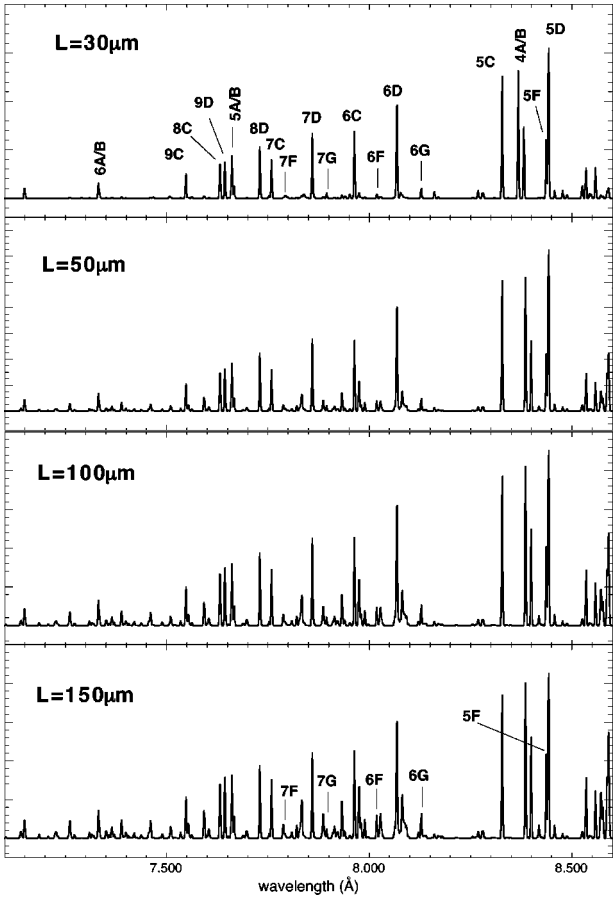

FIG. 6. CR spectra with escape factors for Mg-, Na-, Ne-, F-, and O-like Cu ions computed for $T_e=250$ eV, $N_e=10^{21}$ cm^{-3}, and different plasma diameters. The Ne-like Cu^{19+} lines have been labeled in the upper panel, all line feature have been given a Gaussian profile with a 3.0 m Å FWHM.

C. Hot electron populations

We now study the effect on our spectral models of the inclusion of a small distribution of hot electrons, both with and without escape factors. The dependence of the synthetic spectrum (including Cu^{21+} to Cu^{17+}) on hot electron fraction for the optically thin case is shown in Fig. 7. The simulations assume $T_{\rm bulk}=200$ eV, $N_e=10^{21}$ and 10^{22} cm^{-3}, and $T_{\rm hot}=5$ keV, conditions that are typical of the Nd:glass and Ti:sapphire experiments in the present work. The F-like transitions labeled by greek letters in Fig. 7 are defined in Ref. [23]. The results show a dramatic enhancement of the F-like emission relative to the Ne-like emission features as the hot electron fraction goes from 0 to 5.0×10^{-5} of the bulk population. Looking at the case of $N_e=1.0\times10^{21}$ cm^{-3} (left), the average charge of the ion distribution is shifted only slightly by the inclusion of small fractions ($f_{\rm hot}\leqslant10^{-5}$) of hot electrons, i.e., $\langle Z\rangle=18.76$, 18.77, and 18.84 for $f=0$, 10^{-6}, and 10^{-5}, respectively. For hot electron populations $f_{\rm hot}>10^{-5}$ the increase is larger, with $\langle Z\rangle=19.14$ for $f_{\rm hot}=5\times10^{-5}$. The escape factors discussed in Sec. IV B (for $L=150$ μm) shifted the ionization state distribution to a more highly charged equilibrium by an amount comparable to the shift caused by the $f_{\rm hot}=5\times10^{-5}$ hot electron population, i.e., ~0.4 electrons. For smaller plasma diameters, the effect of the escape factors on the ionization state of the plasma is comparable to the effect of the smaller hot electron populations, a shift of ~0.2 electrons higher. One observes in Fig. 7 that by increasing the density by an order of magnitude, the effect of the hot electrons is somewhat mitigated. This is seen particularly in the relative strengths of the $6D$ and α transitions, and the $6C$ and η transitions. There is no obvious enhancement of any O-like lines in the left panel of Fig. 7 ($N_e=10^{21}$ cm^{-3}), this is because the O-like fractional population, although increased to 4.4×10^{-3} when $f_{\rm hot}=10^{-5}$ from 2.6×10^{-4} when $f_{\rm hot}=0$, it is still quite small and O-like lines show up only weakly. In the right panel, the increase in electron density raises the fraction of O-like ions present by a factor of 2 for all values of $f_{\rm hot}$, but the O-like lines are still too weak for $T_{\rm bulk}=200$ eV, $f_{\rm hot}=5\times10^{-5}$ to be seen in Fig. 7.

Figure 8 shows the same comparison as in Fig. 7, now with escape factors included in the calculation, in this case a plasma diameter of 30 μm has been assumed. By the standards of the discussion in Sec. IV A and above, this dimension is small; however, for $N_e=10^{22}$ cm^{-3} this size is still large enough to cause appreciable self-absorption of some of the Ne-like lines. The relative strengths of lines within the Ne-like charge state are unaffected by the presence of the hot electrons, which lets us deconvolve the enhancement of ionization balance due to hot electrons from the increased average charge state that also results from the inclusion of escape factors. Opacity effects perturb the nC and nD series in the Ne-like ion differently than the nA, B, F, and nG series, thus, the ratio of F-like to Ne-like ion abundance and the relative strengths of Ne-like Rydberg transitions let us assess the relative importance of opacity effects and hot electron populations. Simulations show that there is little difference in any of these results for $T_{\rm hot}$ going from 2–10 keV.

V. PLASMA ANALYSIS

A. Type I plasmas

Figure 9 compares two simulations for a 15-ns pulse Nd:glass LPP spectrum computed with (top) and without (bottom) self-absorption. For the simulation, an isothermal, spherical plasma is assumed with a diameter of 150 μm, $N_e=1.0\times10^{21}$ cm^{-3}, and $T_{\rm ion}=T_e=250$ eV; the theoretical traces have both been normalized to the well-resolved $5C$ line. The laser intensity on target is $\approx7.5\times10^{11}$ W/cm^2, the laser spot size is ≈300 μm. The assumed plasma diameter for the escape factor calculation is probably a factor of 2 smaller than the x-ray emitting plasma volume; this is felt to be reasonable for an isothermal, homogenous approximation to the physical plasma. The observed data are time integrated, and of course, the plasma from the untamped target will have both strong temperature and density gradients. However, the persistence of the Ne-like ion across a range of plasma temperatures, and the insensitivity of the relative strengths of the Ne-like line features to changes in temperature and density (Figs. 4 and 5) means that our assumed plasma conditions are a good representation of the average plasma state. One sees that the calculation with self-

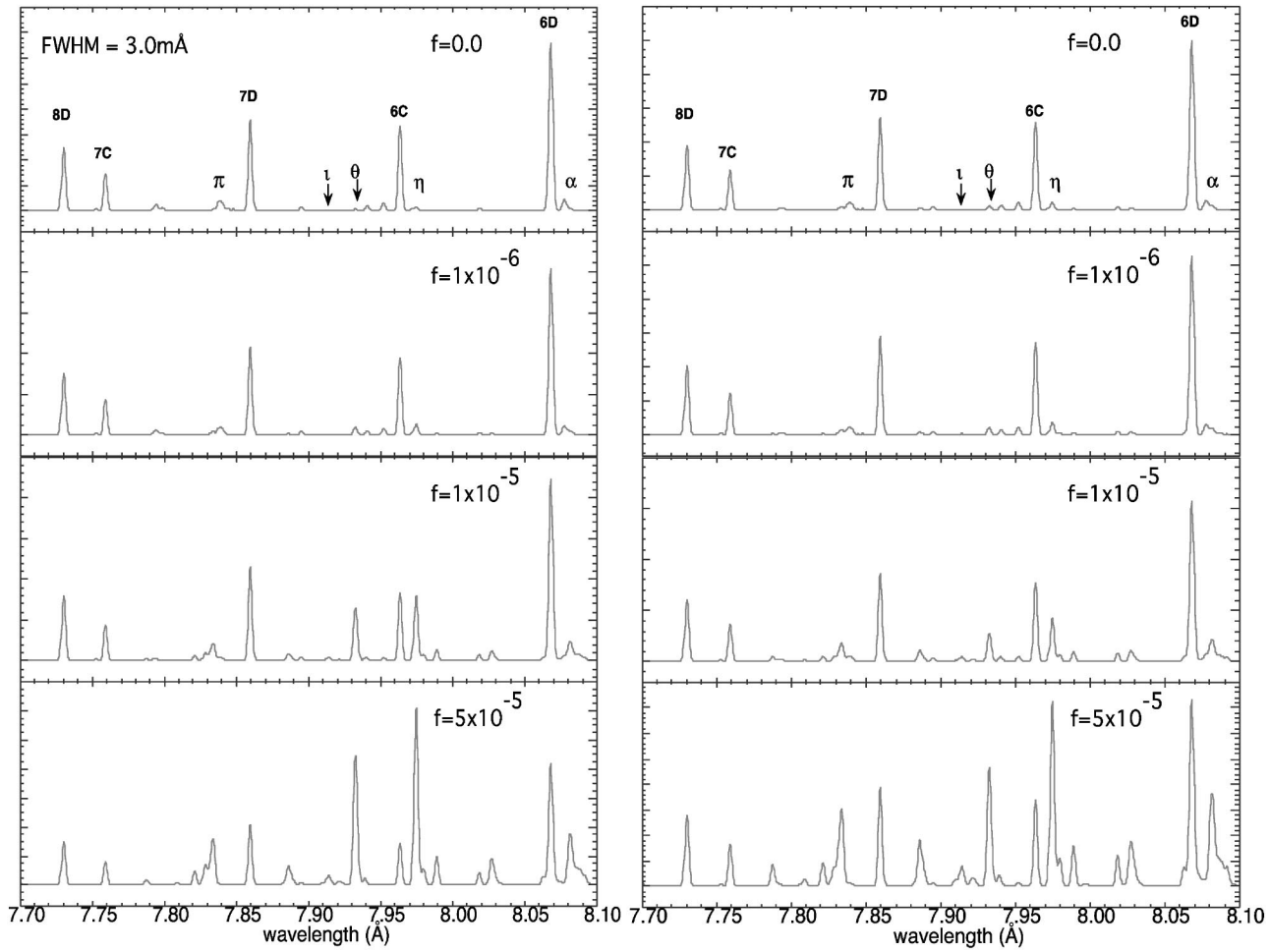

FIG. 7. CR models for O-like to Mg-like copper ions with $T_{\text{bulk}}=200$ eV, $N_e=1.0\times10^{21}$ (left) and 1.0×10^{22} cm^{-3} (right), and increasing hot electron ($T_{\text{hot}}=5$ keV) fraction (from top to bottom), as labeled in the figure.

absorption does a better job of reproducing the $4A$, $4B$, $5F$, and $5D$ relative intensities compared to the optically thin model; this is because the intensities of the $5C$ and $5D$ lines are strongly affected by the escape factors. For plasma diameters $L<150$ μm, the $5D$ and $6D$ lines are too strong, and the $4B$ line is too weak. In both calculations, the $6D$ line is overestimated, although the relative intensity of both $6C$ and $6D$ are closer to the data for the calculation with escape factors. This suggests that there may be more self-absorption in the high-n lines than we are predicting with our simple model. $4B$ line is too weak. In both calculations, the $6D$ line is overestimated, although the relative intensity of both $6C$ and $6D$ are closer to the data for the calculation with escape factors. This suggests that there may be more self-absorption in the high-n lines than we are predicting with our simple model. The simulation in Fig. 9 overall shows very good agreement for the Ne-like Cu^{19+} features and the F-like Cu^{20+} features η, ζ, ε, and α. For a 50 or 100 μm plasma diameter, the F-like features are always underpredicted. There are two bunches of $2p$-$6d$ Na-like Cu^{18+} and $2p$-$4d$ O-like Cu^{21+} features between 8.16 and 8.32 Å that are underpredicted. Given the time-integrated nature of the observations and our steady-state simulations, we cannot account for emission from the plasma that occurs when conditions are far from the average conditions that we are modeling. Variation of the set of parameters in the upper panel of Fig. 9 is discussed in the paragraph below.

In the simulations, we find that changing L from 50 to 150 μm causes the strength of the $5D$ line to be reduced by $\approx12\%$, while the strengths of the α and η features are increased by $\approx33\%$. These two criteria, the strength of the $5D$ line and the strengths of the α and η F-like transitions, are optimized to give us the resulting plasma conditions. For the simulation in Fig. 9, an equally satisfactory fit to the data is achieved for $T_e=300$ eV, $N_e=5\times10^{20}$ cm^{-3}, and an assumed $L=150$ μm. The resulting $\langle Z\rangle$ for $T_e=300$ eV, $N_e=5\times10^{20}$, $L=150$ μm, is very close to that for the simulation in the upper panel of Fig. 9 being 0.05 electrons more ionized, however, the hotter, lower-density calculation does have twice as much O-like Cu^{21+} present. For $T_e=200$ eV, the F-like features are always too weak. For a density $N_e\geqslant5\times10^{21}$ cm^{-3}, there is too much absorption on all Ne-like lines even for an assumed L as small as 50 μm, and for $N_e\geqslant10^{22}$, in a calculation with escape factors, the F-like and O-like transitions form a veritable forest of lines that looks nothing like the data. Thus, the plasma electron temperature is known to within 50 eV, and the electron density is seen to be within a factor of two of the critical density for a 1.055-μm laser.

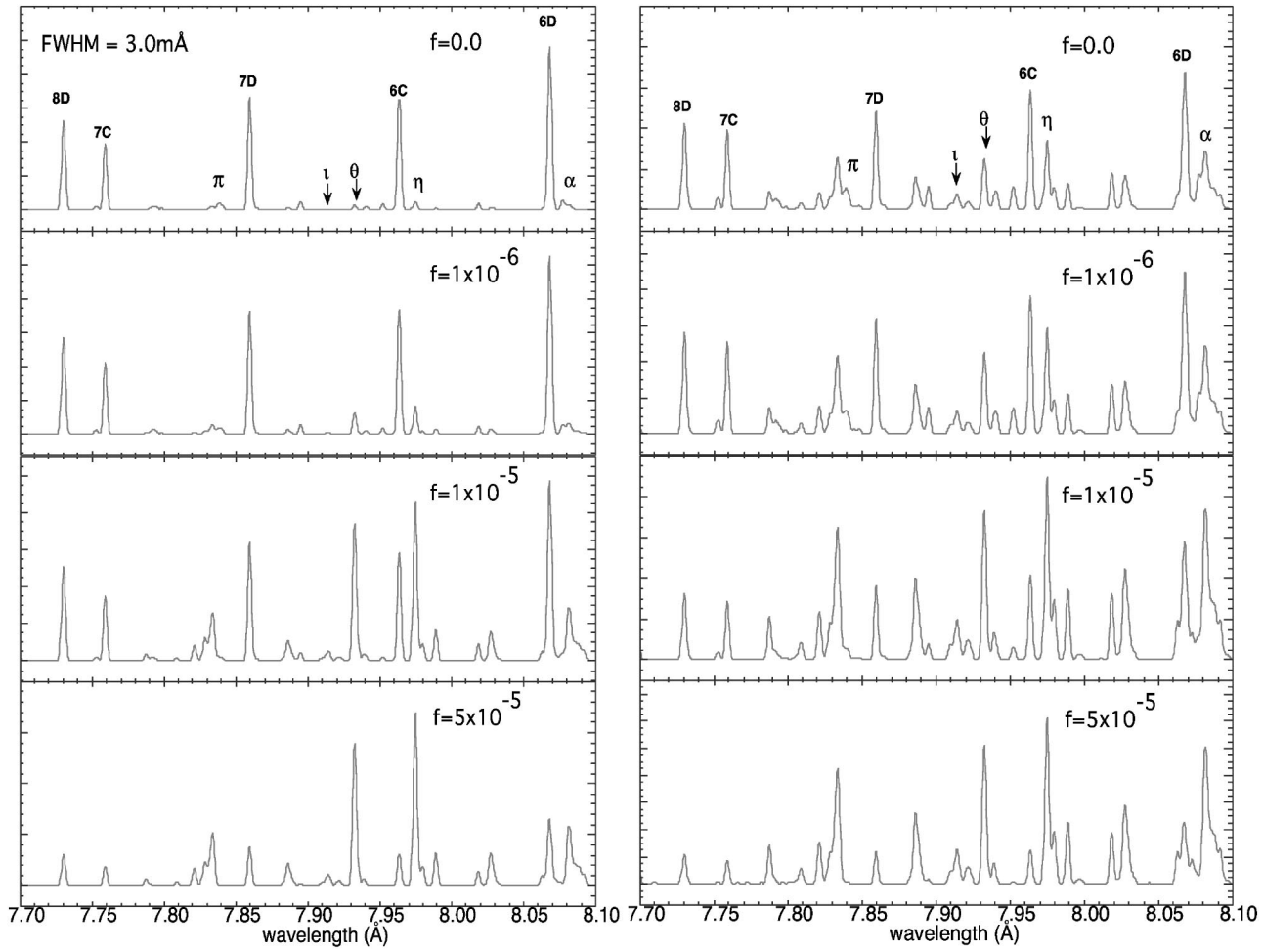

FIG. 8. CR models for O-like to Mg-like copper ions with $T_{\mathrm{bulk}}=200$ eV, $N_e=1.0\times10^{21}$ (left) and 1.0×10^{22} cm^{-3} (right), computed with escape factors for all transitions ($L=30$ μm, $T_{\mathrm{ion}}=T_e$) and increasing hot electron ($T_{\mathrm{hot}}=5$ keV) fraction (from top to bottom), as labeled in the figure.

In Fig. 10, we compare data from a type I LPP spectrum produced by moving the focusing lens 5 mm from the position of best focus with simulations done at $T_e=200$ eV, $N_e=10^{21}$ cm^{-3} with and without optical depths. The contrast between the data in Figs. 9 and 10 shows that reducing the plasma electron temperature by defocusing the laser suppresses the F-like (η, ζ, ε, and α) and O-like lines. In this case, the lower-temperature simulation with escape factors included does a good job of reproducing the correct strength of the F-like features relative to the Ne-like lines. We also find that the $5F$, $6F$, and $6G$ lines are enhanced relative to the $5C$, $6C$, and $6D$ lines beyond what the optically thin model predicts (see Sec. IV B and Fig. 6). The behavior of the $5F$, $6F$, and $6G$ lines further supports the choice of plasma conditions in our simulations. The simulations for type II and type III LPPs, discussed in the next sections, require consideration of a hot electron population in addition to optical depths.

B. Type II plasmas

Figure 11 shows five spectra taken from high-contrast type II Cu LPPs. The lens has been shifted in each shot from best focus (bottom trace) to -1.8 mm from best focus (top trace), thus reducing the plasma temperature going from bottom to top. This is reflected by the gradual disappearance of O-like and F-like features, and the dominance of the Ne-like Cu^{19+} lines. The intensity of the laser on target is $I_{\mathrm{main}}=10^{16}$, 3.3×10^{15}, 2×10^{15}, 10^{15}, and 10^{14} W/cm^2, respectively. The diameter of the x-ray emitting plasma volume in these shots ranges from 100–150 μm to 300–500 μm as the laser is defocused. The expected density in these plasmas is within a factor of 2 of the critical density for 1.055 μm light, i.e., 0.5×10^{21}–2.0×10^{21} cm^{-3}; however, our calculations can also find good agreement with the observations for densities as high as $N_e=10^{22}$ cm^{-3}. Hot electrons are seen to be present, as will be discussed below. The presence of a laser prepulse can enhance the hot electron population [12,13], but for the present work the difference between the high- and low-contrast type II spectra is not enough to demonstrate this conclusively. At present, we have no ability to reduce the first type of prepulse described for the ''Neodym'' laser (Sec. II), or to increase the overall contrast between the aggregate prepulse and the main laser pulse.

Figure 12 compares data from a type II LPP with simulations that include both hot electrons and escape factors. For

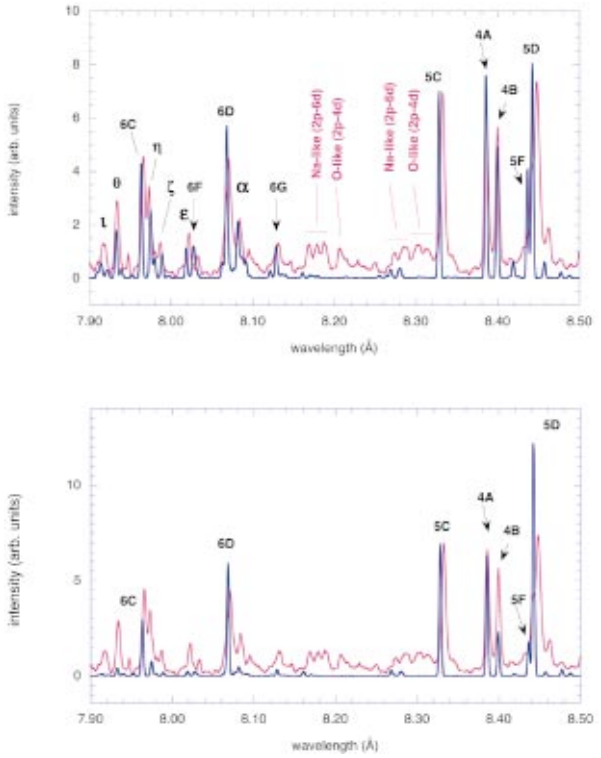

FIG. 9. (Color) Type I LPP spectrum (15-ns pulse with $E_{\text{pulse}}=8$ J), data (pink) have been overlaid with a CR spectra (blue) computed with (top) and without (bottom) escape factors ($T_e=250$ eV, $N_e=10^{21}$ cm^{-3}, for escape factors: $T_{\text{ion}}=250$ eV, $L=150$ μm).

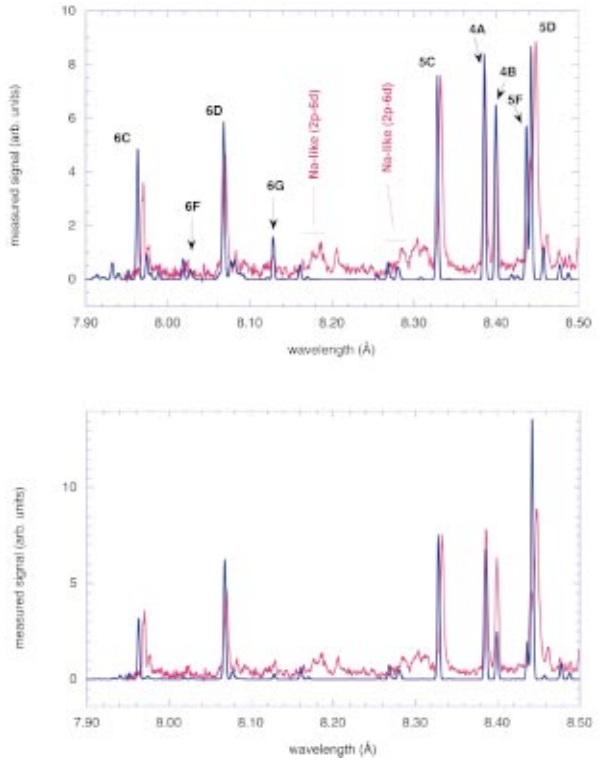

FIG. 10. (Color) Type I LPP spectrum (15-ns pulse with $E_{\text{pulse}}=8$ J, lens moved 5 mm from best focus), data (pink) have been overlaid with a CR spectra (blue) computed with (top) and without (bottom) escape factors ($T_e=200$ eV, $N_e=10^{21}$ cm^{-3}, for escape factors: $T_{\text{ion}}=200$ eV, $L=150$ μm).

this case, the data are from high-intensity (10^{16} W/cm^2), low-contrast ($I_{\text{main}}/I_{\text{pp}}=10^5$) shots. The simulations shown are for an optically thin plasma with $T_e=400$ eV and $N_e=10^{21}$ cm^{-3} (middle), and for a plasma with $T_e=350$ eV, $N_e=10^{21}$ cm^{-3}, escape factors included with an assumed plasma diameter of 50 μm and $f_{\text{hot}}=10^{-5}$ (bottom). The two simulations give comparable reproductions of the data; the higher-temperature, optically thin run matches the strength of the F-like and, in particular, the O-like lines better. There is little difference in the Ne-like spectrum for runs with and without escape factors for $T_e \geqslant 350$ eV because the fraction of Ne-like ions present at such temperatures is strongly reduced, thus the absorber-ion density is not enough to give rise to strong opacity effects for $L \leqslant 100$ μm. Given the 100 μm focal-spot diameter in these experiments, the size of the x-ray emitting plasma is less than this. For the F-like spectrum, the θ, η, and α lines have the correct relative heights for $T_e=400$ eV and $f_{\text{hot}}=0$ and for $T_e=350$ eV and $f_{\text{hot}}=10^{-5}$. The ratio of the F-like to Ne-like lines is better in Fig. 12 for the optically thin simulation, giving $f_{\text{hot}}=10^{-5}$ as an upper limit. However, for $T_e=350$ eV and $f_{\text{hot}}=0$, the F-like lines are far too weak compared to the data in Fig. 12, suggesting some hot electrons are present. Finally, the O-like $2p$-$4d$ transitions labeled in Fig. 12 are better reproduced by the $T_e=400$ eV, optically thin simulation. A good fit to the observed data can also be achieved with $T_e=300$ eV, $N_e=10^{22}$, and $f_{\text{hot}}=10^{-5}$ (not shown in Fig. 12). The addition of any escape factors ($L \geqslant 20$ μm) at this density creates a spectrum with many more weak lines between the main features than are actually seen in the measured spectra. As shown in Fig. 7, the increased bulk electron density of $N_e=10^{22}$ cm^{-3} mitigates the effect of the hot electrons making $f_{\text{hot}}=10^{-5}$ plausible. However, given the laser prepulse, this density is very high for the blow-off plasma from our Cu targets. Further experiments were done looking at temperature- and density-sensitive lines in the *K*-shell spectra of Mg and Al; conditions similar to those described above, $T_e=350$–400 eV, $N_e \approx 10^{21}$ cm^{-3} were found.

Figure 13 shows data from a type II LPP shot with high contrast between the prepulse and the main pulse. The focusing lens has been shifted slightly from the position of best focus, so the intensity, $I=3.3\times10^{15}$ W/cm^2, and consequently the plasma bulk electron temperature is slightly lower than in Fig. 12. The data in this figure extend to shorter wavelengths than in Fig. 12, and very high-n members of the nC and nD series in Ne-like Cu^{19+}, for which only calculated transition wavelengths were listed in Ref. [23], can be seen. Also, despite the prediction in Ref. [23] that the $6A,B$ and $7A,B$ lines would be difficult to observe due to large branching ratios towards autoionization, we can clearly identify features in the data at the right wavelengths, which also have the correct relative intensities in the simulation. F-like Cu^{20+} transitions of the form $2p$-$8d$, $2p$-$7d$, and $2s$-$5p$ give rise to very strong features between 7.25 and 7.40 Å, each of which is composed of 2–8 unresolved lines. Our simulation does not have the CR intensities computed for

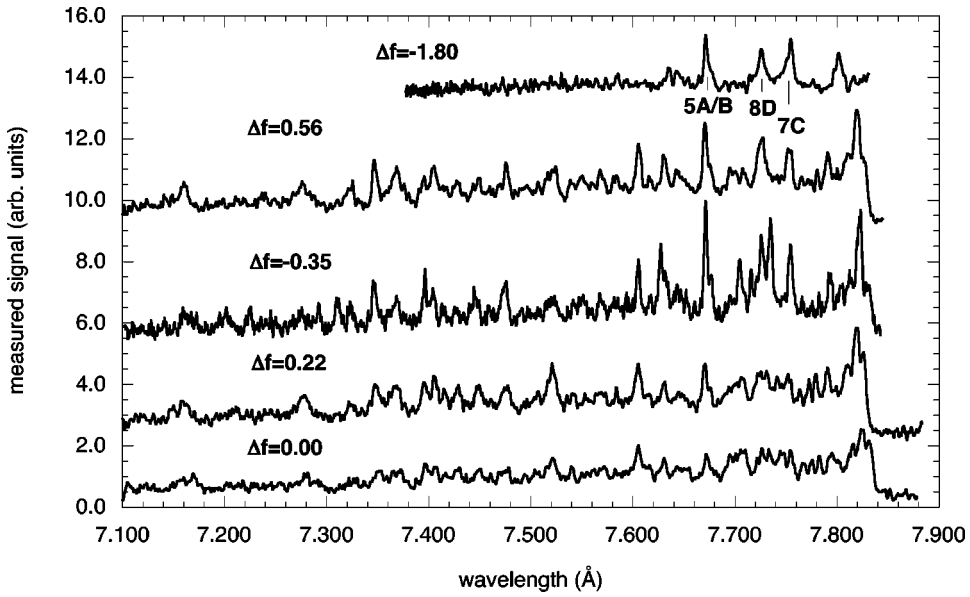

FIG. 11. Type II (ps-pulse) LPP spectra where the laser focus has been changed, with $\Delta f = 0.0$, 0.22, 0.35, 0.56, and 1.8 mm, from bottom to top, respectively. All of these shots were in the high contrast $I_{\text{main}}/I_{\text{pp}} \sim 10^7$ regime.

transitions with $n \geqslant 10$ for any isoelectronic sequence, so the simulation in Fig. 13 does not show any of the very high-n nC and nD Ne-like features that are labeled; fortunately, the $n=2$ to $n=6,7,8$ transitions for the F- and O-like ions do fall in this spectral window. The relative intensities of the F- and O-like lines to each other, and to the relatively weak Ne-like lines, do not demonstrate sensitivity to hot electron populations. The strength of the F- and O-like lines in this spectrum is strongly dependent on the inclusion of escape factors in the simulation. We find the best agreement with the observations for simulations with L between 30–50 μm. In this case, with the lens slightly defocused, the x-ray emitting plasma has a diameter between 150–200 μm. We find the best agreement with the data for a simulation that has a density of $N_e = 10^{22}$ cm^{-3}, this is based on the strength of many weak F- and O-like lines that are only visible in the simulation for $N_e = 10^{22}$ cm^{-3} (compare the middle and bottom traces in Fig. 13). Since the data in Fig. 13 are from shots with high contrast between the prepulse and main laser pulse, it is possible that there is less of a preformed blow-off plasma, and thus higher densities are achieved. We cannot, at present, claim that this spectrum offers unambiguous evidence of hot electron populations, but our simulations do indicate that an upper limit on the hot electron fraction is 1×10^{-5}.

C. Type III plasmas

Figure 14 shows data from a type III plasma produced by a 60-fs Ti:sapphire laser pulse ($E_{\text{pulse}} = 800$ mJ, $I = 10^{18}$ W/cm^2). The synthetic spectra for the Ne-, F-, and O-like lines from the CR model at $T_e = 200$ eV, $N_e = 10^{22}$ cm^{-3} including a population of 5-keV electrons ($f_{\text{hot}} = 5 \times 10^{-5}$) are also shown in Fig. 14, each line has

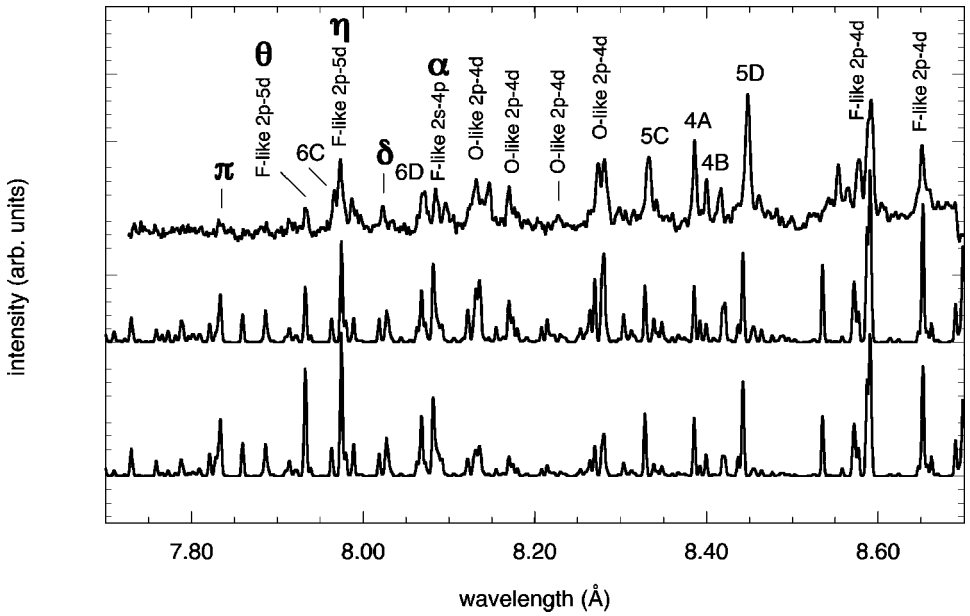

FIG. 12. High-intensity (10^{16} W/cm^2), type II (ps-pulse) LPP spectrum (top) with the laser at best focus and low contrast between the main pulse and the prepulse ($I_{\text{main}}/I_{\text{pp}} = 10^5$). Also shown are two simulations with (middle) $T_e = 400$ eV, $N_e = 10^{21}$ cm^{-3}, and $f_{\text{hot}} = 0$ and with (bottom) $T_e = 350$ eV, $N_e = 10^{21}$ cm^{-3}, $f_{\text{hot}} = 10^{-5}$ and escape factors included ($L = 50$ μm).

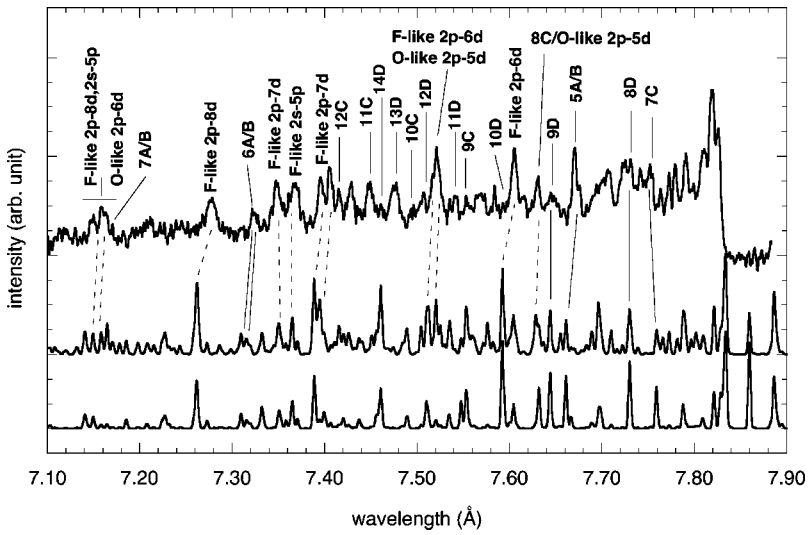

FIG. 13. High-intensity (3.3×10^{15} W/cm^2), type II (ps-pulse) LPP spectrum (top) with the focusing lens shifted 0.22 mm from best focus and high contrast between the main pulse and the prepulse ($I_{\rm main}/I_{\rm pp}=10^7$). Also shown is a simulation with $T_e=300$ eV, $N_e=10^{22}$ cm^{-3}, $f_{\rm hot}=10^{-5}$ and with escape factors included ($L=30$ μm, middle), and a spectrum calculated with $T_e=300$ eV, $N_e=10^{21}$ cm^{-3}, $f_{\rm hot}=10^{-5}$ and escape factors ($L=50$ μm, bottom).

been give a Gaussian shape with a 3.5 mÅ full width at half maximum (FWHM). From the agreement between the calculated and observed transition wavelengths in Fig. 14, it is clear that the measured wavelengths in this plasma are less accurate than in the Nd:glass LPPs. Further, the systematic growth of the difference between observed and calculated wavelengths, indicated by the dashed lines in Fig. 14, suggests that the dispersion in this case may not be well calculated. This may explain why the higher-n ($n\geqslant7$) lines in the Ne-like spectrum do not appear in the data. The relative intensities of the $5D$, $5C$, $4A$, and $4B$ transitions show good agreement with the observed lines. The relative strengths of these lines are unaffected by the presence of the hot electrons. The laser spot size in these experiments was ≈30 μm, giving rise to an x-ray emitting plasma with a diameter of 30–100 μm, a size too small for opacity effects to play a role. The strength of the F-like features α, η, and θ are in good agreement with each other and with the Ne-like features in the simulation. For a smaller hot electron population, the F-like lines are underestimated (see evolution in Figs. 7 and 8). The bulk temperature must be as high as 350 eV in order to see similar Ne- to F-like line ratios, however, the presence of O-like transitions between 8.16 and 8.32 Å would also be strongly enhanced, and they are clearly not seen in the data shown in Fig. 14. This is a bulk temperature too high for the given laser energy, thus the presence of hot electrons in the type III spectrum is confirmed.

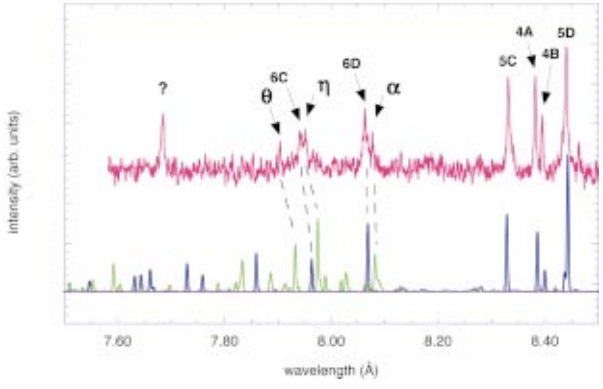

FIG. 14. (Color) Data from a type III LPP (60-fs pulse, $I=10^{18}$ W/cm^2) and calculated CR spectra for Ne- (blue), F-like (green), and O-like (purple) Cu ions. The synthetic trace is from an optically thin calculation with $T_{\rm bulk}=200$ eV, $N_e=10^{22}$ cm^{-3}, $T_{\rm hot}=5.0$ keV, $f_{\rm hot}=5\times10^{-5}$.

VI. DISCUSSION

Recently, a thorough work was carried out modeling the effect of hot electrons on the L-shell spectra of highly charged Kr ions emitted following the irradiation of atomic clusters in supersonic gas jets [22]. In that work, it was found that for similar irradiation conditions to those used in the present type III experiments, a Kr plasma is produced with $T_e=300$–400 eV, $N_e=1$–2×10^{21} cm^{-3}, and a population of hot electrons with a Gaussian energy distribution $E_{\rm hot}$ centered at 5.0 keV that is 2–4 % of the bulk population. Differences in the electron heat conductivity of the gas-cluster plasma and the solid-target plasma of the present work make direct comparison of the derived bulk temperatures meaningless. The difference in derived electron densities, an order of magnitude, is due to the different initial densities of the gas targets in Ref. [22] and the solid targets of the present work. In Ref. [22], the Gaussian EDF was chosen since the reduced thermal conductivity of the Kr-cluster plasma leads to a longer thermalization time for the hot electrons compared to their thermalization in the bulk copper targets of the present work. Calculations in Ref. [22] show that the bi-Maxwellian EDF with a cold bulk temperature and a small hot population has the same effect on electron impact excitation rates as an EDF with a cold bulk temperature and a Gaussian hot electron population that is ≈2–3 orders of magnitude larger than the hot Maxwellian population. Thus, the derived hot electron fraction for the type III LPPs of the present work are consistent with the hot electron populations found for the same laser-irradiation conditions in Ref. [22].

The work of Young *et al.* in Ref. [5] is the only other work we are aware of that looks at L-shell emission from solid targets irradiated by subpicosecond lasers. In that work,

for laser intensities lower than those in our type III experiments by a factor of 3, space and time integrated spectra give bulk plasma temperatures ranging from 250–430 eV, and near solid densities. For those experiments, the laser wavelength was 400 nm (2ω for a Ti:sapphire laser), a factor of 2 shorter than in the present work. The laser-pulse duration in Ref. [5] was 130 fs, twice as long as in the present work, and the contrast between the prepulse and the main laser pulse was much sharper than in the present work as a consequence of working with 2ω light. Differences in the level of prepulse and the laser-target coupling at the different wavelengths used make further direct comparisons of these two experiments difficult. With the poorer contrast ratio of the present work, the lower-density plasma with a hot electron population that we have found is very reasonable. We are unaware of any other investigations of *L*-shell spectra from solid targets irradiated by intense, $I \geqslant 10^{18}$ W/cm^2, subpicosecond lasers.

VII. CONCLUSION

We have observed x-ray lines from high-n transitions in near neonlike copper ions from three different laser-produced plasmas. We emphasize that the $n=2$ to $n=5,6,7,8$ transitions in F-like Cu^{20+} and O-like Cu^{21+} have not been examined in detail before. The effects of increasing electron density on both plasma self-absorption and inner-shell excitation due to hot electrons have been demonstrated: absorption is strongly enhanced with increasing density while the effect of the hot electrons is reduced. We show that for the case of ns-scale LPPs, treating opacity effects, in the present work with escape factors, is necessary for reproducing the correct relative intensities of high-n Ne-like Cu^{19+} lines. For the irradiation conditions used here, $I \approx 10^{12}$ W/cm^2, we find plasma electron temperatures from 250–300 eV and electron densities 0.5×10^{21}–1.0×10^{21} cm^{-3}. The actual x-ray emitting plasma has a diameter of the order of 300 μm, we find an adequate description for the escape factors assuming a homogeneous, isothermal plasma with a diameter $L=150$ μm. The escape factors are a sensitive lever on the ion charge state distribution; only with escape factors can the F- and O-like ion populations be adequately enhanced. For ps-scale LPPs, we find that high-temperature, $T_e=400$ eV, optically thin simulations with $N_e=10^{21}$ cm^{-3} reproduce well the observed spectra for high-intensity, $I\approx10^{16}$ W/cm^2, laser shots with low contrast between the laser prepulse and the main laser pulse. We find an upper limit of $f_{\rm hot}\leqslant10^{-5}$ in these spectra. For the ps-scale shots with the laser at its best focus, the scale of the x-ray emitting plasma was ≈100 μm; for the highest intensities, these plasmas are too hot and small for opacity effects to be significant on the Ne-like Cu^{19+} transitions. For ps-scale LPPs with higher contrast between the prepulse and the main laser pulse, we find that simulations with electron densities as high as $N_e=10^{22}$ cm^{-3}, and both hot electron populations and escape factors, are necessary to match the observed F- and O-like copper ion spectra. In this case, the laser has been defocused, and the 150–200 μm diameter x-ray emitting plasma is well simulated with an assumed diameter of 30–50 μm for a homogeneous, isothermal plasma. The strength of the $n=2$ to $n=5,6,7,8$ spectra in F- and O-like copper ions is particularly sensitive to a combination of the assumed plasma diameter and higher plasma electron densities ($N_e=10^{22}$ cm^{-3}). These higher densities are found in simulations of shots with high contrast between the laser prepulse and the main pulse. We cannot, at present, control the contrast between the prepulse and main laser pulse well enough to demonstrate the dependence of the hot electron population on this parameter. In spectra from a 60-fs LPP, for a laser intensity $I=10^{18}$ W/cm^2, we find a bulk electron temperature $T_e=200$ eV, and an electron density $N_e\approx10^{22}$ cm^{-3}. The enhancement of the F-like ion population is clearly seen, indicating that a hot electron population $f_{\rm hot}\approx2\times10^{-5}$–$5\times10^{-5}$ is present.

ACKNOWLEDGMENTS

This work was performed under the auspices of the U.S. Department of Energy by University of California Lawrence Livermore National Laboratory under Contract No. W-7405-Eng-48. The work of A.Y.F. was partly supported by a grant from the Italian Ministry of Foreign Affairs through the Landau Network-Centro Volta Fund. This work was also partly supported by ISTC project N 2155.

[1] J. Lindl, Phys. Plasmas **2**, 3933 (1995).
[2] M.M. Murnane, H.C. Kapteyn, and R.W. Falcone, Phys. Rev. Lett. **62**, 155 (1989).
[3] P. Audebert, J.P. Geindre, A. Rouse, F. Falliès, J.-C. Gauthier, A. Mysyrowicz, G. Grillon, and A. Antonetti, J. Phys. B **27**, 3303 (1994).
[4] D.F. Price, R.M. More, R.S. Walling, G. Guethlein, R.L. Shepherd, R.E. Stewart, and W.E. White, Phys. Rev. Lett. **75**, 252 (1995).
[5] B.K.F. Young, B.G. Wilson, D.F. Price, and R.E. Stewart, Phys. Rev. E **58**, 4929 (1998).
[6] K.B. Fournier, B.K.F. Young, S.J. Moon, M.E. Foord, D.F. Price, R.L. Shepherd, and P.T. Springer, J. Quant. Spectrosc. Radiat. Transf. **71**, 339 (2001).
[7] S. Bastiani, A. Rousse, J.P. Geindre, P. Audebert, C. Quoix, G. Hamoniaux, A. Antonetti, and J.-C. Gauthier, Phys. Rev. E **56**, 7179 (1997).
[8] Th. Schlegel, S. Bastiani, L. Grémillet, J.-P. Geindre, P. Audebert, J.-C. Gauthier, E. LeFebvre, G. Bonnaud, and J. Delettrez, Phys. Rev. E **60**, 2209 (1999).
[9] W. L. Kruer, *The Physics of Laser Plasma Interactions* (Addison-Wesley, Redwood City, CA, 1988).
[10] F. Brunel, Phys. Rev. Lett. **59**, 52 (1987); Phys. Fluids **31**, 2714 (1988).
[11] D. Gordon *et al.*, Phys. Rev. Lett. **80**, 2133 (1998).
[12] A. Rousse, P. Audebert, J.P. Geindre, F. Falliès, J.-C. Gauthier, A. Mysyrowicz, G. Grillon, and A. Antonetti, Phys. Rev. E **50**, 2200 (1994).
[13] J.-C. Gauthier, S. Bastiani, P. Audebert, J.P. Geindre, A.

Rousse, C. Quoix, G. Grillon, A. Mysyrowicz, A. Antonetti, R. Mancini, and A. Shlyaptseva, Proc. SPIE **3157**, 52 (1997).
[14] J. Abdallah, Jr., A.Ya. Faenov, D. Hammer, S.A. Pikuz, G. Csanak, and R.E.H. Clark, Phys. Scr. **53**, 705 (1996).
[15] J. Abdallah, Jr., R.E.H. Clark, A.Ya. Faenov, L. Karpinski, S.A. Pikuz, V.M. Romanova, M. Sadowski, M. Scholz, and A. Szydlowski, J. Quant. Spectrosc. Radiat. Transf. **62**, 85 (1999).
[16] J. Abdallah, Jr., A.Ya. Faenov, T.A. Pikuz, M.D. Wilke, G.A. Kyrala, and R.E.H. Clark, J. Quant. Spectrosc. Radiat. Transf. **62**, 1 (1999).
[17] J. Abdallah, Jr., A.Ya. Faenov, I.Y. Skobelev, A.I. Magunov, T.A. Pikuz, T. Auguste, P. D'Oliveira, S. Hulin, and P. Monot, Phys. Rev. A **63**, 032706 (2001).
[18] S. Bastiani, P. Audebert, J.P. Geindre, Th. Schlegel, J.-C. Gauthier, C. Quoix, G. Hamoniaux, G. Grillon and A. Antonetti, Phys. Rev. E **60**, 3439 (1999).
[19] G.C. Junkel-Vives *et al.*, Phys. Rev. A **64**, 021201(R) (2001).
[20] G.C. Junkel-Vives *et al.*, J. Quant. Spectrosc. Radiat. Transf. **71**, 417 (2001).
[21] G.C. Junkel-Vives *et al.*, Phys. Rev. E **65**, 036410 (2002).
[22] S.B. Hansen *et al.*, Phys. Rev. E **66**, 046412 (2002).
[23] K.B. Fournier *et al.*, J. Phys. B **35**, 3347 (2002).
[24] V.S. Belyaev, V.I. Vinogradov, A.S. Kyrilov, A.P. Matafonov, A.V. Pakulev, and V.E. Yashin, Quantum Electron. **30**, 229 (2000).
[25] T. Auguste, P. D'Oliveira, S. Hulin, P. Monot, J.J. Abdallah, A.Y. Faenov, I.Y. Skobelev, A.I. Magunov, and T.A. Pikuz, Pis'ma Zh. Eksp. Teor. Fiz. **72**, 54 (2002) [JETP Lett. **72**, 38 (2000)].
[26] D. Strickland and G. Mourou, Opt. Commun. **56**, 219 (1985).
[27] M.D. Perry and G. Mourou, Science **264**, 917 (1994).
[28] A.Ya. Faenov, S.A. Pikuz, A.I. Erko, B.A. Bryunetkin, V.M. Dyakin, G.V. Ivanenkov, A.R. Mingaleev, T.A. Pikuz, V.M. Romanova, and T.A. Shelkovenko, Phys. Scr. **50**, 333 (1994).
[29] T.A. Pikuz, A.Ya. Faenov, S.A. Pikuz, V.M. Romanova, and T.A. Shelkovenko, J. X-Ray Sci. Technol. **5**, 323 (1995).
[30] B.K.F. Young *et al.*, Rev. Sci. Instrum. **69**, 4049 (1998).
[31] M. Klapisch, Comput. Phys. Commun. **2**, 239 (1971).
[32] M. Klapisch, J. Schwob, B. Fraenkel, and J. Oreg, J. Opt. Soc. Am. **67**, 148 (1977).
[33] A. Bar-Shalom, M. Klapisch, and J. Oreg, Phys. Rev. A **38**, 1773 (1988).
[34] J. Oreg, W.H. Goldstein, M. Klapisch, and A. Bar-Shalom, Phys. Rev. A **44**, 1750 (1991).
[35] W. Lotz, Z. Phys. **216**, 241 (1968).
[36] W. Lotz, Z. Phys. **232**, 101 (1970).
[37] E.B. Saloman, J.H. Hubble, and J.H. Scofield, At. Data Nucl. Data Tables **38**, 1 (1988).
[38] T. Holstein, Phys. Rev. **72**, 1212 (1947).
[39] E.E. Fill, J. Quant. Spectrosc. Radiat. Transf. **39**, 489 (1988).
[40] G.V. Brown, P. Beiersdorfer, H. Chen, M.H. Chen, and K.J. Reed, Astrophys. J. Lett. **557**, L75 (2001).